interest, but also it may give a system over-parametrized so that we must keep cautious. This way, we have prepared the isostructural (MgNi) compound in which the Ni(II) ion occupies selectively the "quelated" position. Unfortunately, no signal has been observed by EPR measurement, probably due to the large distortion from the octahedral symmetry (preliminary specific heat studies suggest a large zero-filed splitting of the $^3A_2$ ground term). Nevertheless, an upper limit of g_a/g_b[24] can be assumed by refering to commonly observed g values for the Ni(II) ion in similar environments (varying between 2.1 and 2.4).[22] A least-squares refinement of the limiting curve ($N \rightarrow \infty$) (Figure 7) computed for $g_a/g_b = 1.1$ led to the rational expression

$$\frac{\chi|J|}{Ng^2\beta^2} = \frac{4x + 0.1864x^2 + 1.2084x^3}{3 + 4.7658x + 3.3652x^2 + 8.3403x^3} \quad (7)$$

where $x = |J|/kT$.

The agreement criterion defined as the sum of the squares of the relative deviations is $R = 1.6 \times 10^{-5}$. Using expression 7, the best agreement between theory and experiment (solid line in Figure 5) corresponds to $J = -8.35K$, $g_a = 2.31$, and $g_b = 2.10$. It is to be noticed that the description of the low-temperature susceptibility is not improved by introducing the g alternation. In particular, the experimental data decrease significantly when cooling down to zero by contrast with theoretical ones. Such a discrepancy could result from the local anisotropy effects, not introduced in the above model. Unfortunately, the theoretical treatment of the Heisenberg chain involving two distinct local distortions is not available today.

Anyway, it has been emphasized that a local anisotropy of the Ni(II) ions establishes a preference for the moments to align in a given direction[5] so that an anisotropic exchange model (Ising or XY-type) becomes relevant to analyze the magnetic behavior. Using the Ising model developed in the previous section, we show that the quality of the fit is greatly improved by only taking into account J, g_a, and g_b as adjustable parameters (dashed line in Figure 5); we obtain $J = -8.25K$, $g_a = 2.21$, and $g_b = 2.09$. Note that such a model gives a very good description of the rounded maximum and agrees with the data at lower temperatures. From a close examination, it does not seem necessary to introduce in the fit further parameters. This suggests that the anisotropic exchange model is convenient to describe the competition between anisotropy effects and exchange coupling in the temperature range of interest.

(22) McGarvey, B. R. *Transition Met. Chem. (Weinheim, Ger.)* **1966**, *3*, 89.

Conclusion

We have discussed in this paper the behavior of an $S = 1$ chain characterized by alternating Landē factors. So far, the 1D ferrimagnetic character was related to the presence of two noncompensated spin sublattices. We show, here, that the alternation of Landē factors gives rise to the same divergence of susceptibility when $T \rightarrow 0$ K (ferrimagnetic chains).

Two exchange models were developed to describe the behavior of the $Ni_2(EDTA)(H_2O)_4,2H_2O$ complex, namely the Heisenberg and Ising models.

The former was shown to give a poor agreement with experiment in spite of the consideration of alternating g factors. Clearly, the analysis of the $\chi = f(T)$ variation is greatly improved by using the fully anisotropic (Ising) model. In fact, further effects could be invoked in order to explain the decrease of susceptibility below $T = 10$ K, as for instance magnetic interactions between neighboring chains. Specific heat studies down to 0.1 K have shown that this effect should be negligeable in the present system.[23] Finally, it is to be underlined that the slight inequality between consecutive Ni–Ni distances, related to different bridging carboxilate angles (see Table IV), could result in a J-alternating chain. A complete treatment involving this last effect is in progress.

Acknowledgment. This work was partly supported by the CAICYT and by the "Programme d'actions intêgrées franco-espagnoles".

Registry No. (NiNi), 99687-31-7.

Supplementary Material Available: Listings of structure factor amplitudes (10 pages). Ordering information is given on any current masthead page.

(23) de Jongh, J., private communication.

(24) In agreement with crystal field parameters of the two Ni(II) ions (D = 1030 and 820 cm^{-1} for the "chelated" and "hydrated" site, respectively) the larger g value (g_a) may be associated to the "hydrated" site.

Ultraviolet Resonance Raman Characterization of Photochemical Transients of Phenol, Tyrosine, and Tryptophan

Craig R. Johnson, Michael Ludwig, and Sanford A. Asher*

Contribution from the Department of Chemistry, University of Pittsburgh, Pittsburgh, Pennsylvania 15260. *Received July 26, 1985*

Abstract: Ultraviolet resonance Raman (UVRR) spectra of solutions of phenol, tyrosine, and tryptophan at pH 7 and 12 show Raman bands that are assigned to the photoionization products phenoxy, tyrosyl, and tryptophanyl radicals, respectively. These photoinduced transients are only detected at high laser power densities (high average power, tightly focused, pulsed-laser excitation) when exciting within the $\pi \rightarrow \pi^*$ transitions of the precursor compounds. Each of the radicals show UVRR spectra distinct from their precursors. A pump–probe experiment shows that the phenolate transient (phenoxy radical) produced by the incident laser beam at pH 12 has a lifetime significantly longer than 10 ns. The dependence of the Raman scattering intensity upon incident laser-power density is consistent with a simple model in which the free radical is produced by a monophotonic photoionization process. Saturation effects are also evident at high power densities. Photochemistry, absorption band optical saturation, and nonlinear optical processes are proven and potential impediments for measurements of Raman spectra and excitation profiles with pulsed laser excitation. On the other hand, the facile production and detection of free radical species with UVRR suggest that this technique will be useful in the investigation of radical structure and chemistry.

Several major research efforts,[1-3] in addition to our own, are under way to extend the study of resonance Raman excitation profiles into the ultraviolet and vacuum-ultraviolet[4] spectral regions. Much of this work is directed toward the application of

0002-7863/86/1508-0905$01.50/0

UV resonance Raman (UVRR) spectroscopy to the study of molecular excited states and biologically important molecules. Among the molecules studied by UVRR have been carbon disulfide,[5] ammonia,[6] ethylene,[7] benzene[8,9] and its simple derivatives[10] (toluene, xylene, etc.), the aromatic amino acids,[11-13] polycyclic aromatic hydrocarbons (PAH's),[14] and the peptide backbone model compounds, acetamide and *N*-methylacetamide.[15,16] UVRR spectra of myoglobin,[11] hemoglobin,[17] and cytochrome C[18] have also been reported. The utility of UVRR spectroscopy as a probe of the aromatic amino acid side chains of proteins is now under active investigation.

In this report we describe the facile production and the UVRR detection of photochemical transients using pulsed UV laser excitation. Great care must be taken to avoid photochemical transients and nonlinear optical phenomena if useful UVRR spectra of unperturbed ground-state molecules are to be obtained. On the other hand, new information about the photophysics and photochemistry of a number of important aromatic molecules can be easily obtained from the UVRR spectra of phototransient species.

The ultraviolet photochemistry of the aromatic amino acids and of proteins has been the object of considerable research[19,20] because of the relevance of this area of research to the UV inactivation of enzymes.[21] Although a number of photochemical processes are possible,[19] it is clear that photoionization plays a major role in the photophysics of aromatic molecules. Numerous techniques have been used to study these photoprocesses, including ESR (spin trapping),[22] flash photolysis,[23] and steady-state measurements.[24]

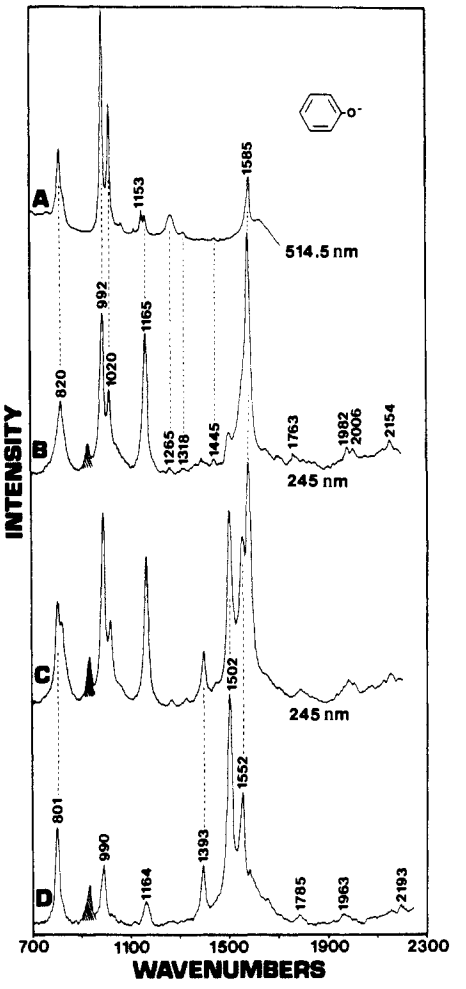

Figure 1. Raman spectra of phenolate ion (pH 12): (A) normal Raman at 514.5-nm excitation with a CW laser (the phenolate concentration is 250 mM, power = 840 mW, spectral bandpass = 2.5 cm^{-1}); (B) UVRR spectrum of a 5 mM phenolate solution at 245-nm excitation using a 20-Hz Nd-Yag laser at 3-mW average power (for this spectrum the laser beam was focused ~10 cm above the sample); (C) same conditions as B but with the laser beam now focused right at the sample (see text for estimates of the power densities for spectra B and C); (D) spectrum of the phenolate transient obtained as the difference spectrum between B and C after appropriate scaling. Perchlorate ion, present as an internal standard in the UV excited spectra, is indicated by shading. The UV spectra were obtained with 15-min scans. Spectral bandpass = 12 cm^{-1}.

We report here the first detection of photoinduced transients of phenol, tyrosine, and tryptophan with UVRR spectroscopy using 270–217-nm excitation. The spectra of these transients are consistent with their assignment as the radicals produced by photoionization. The results suggest that UVRR spectroscopy will provide a new technique for the study of photoionization of proteins as well as the aromatic amino acids.

Experimental Section

Phenol, tyrosine, and tryptophan were obtained from Aldrich and used without further purification. Solutions of each of the compounds were prepared in doubly deionized water or in 0.1 M aqueous NaOH. For some samples $NaClO_4$ was added as an internal intensity standard.[25] The instrumentation used to obtain the UVRR spectra has been described in detail elsewhere.[1] The Quanta Ray Nd-Yag laser was operated at a 20-Hz repetition rate with a pulse width of ca. 4 ns. The samples were recirculated through the laser excitation beam in a quartz capillary or, for the experiments requiring tighter focusing of the beam, through an open-air jet nozzle system. The power density at the sample was altered by adjusting the height of the focusing lens or by placing neutral density filters in the beam. The frequency axes of the spectra were calibrated by referencing the spectra to spectra of acetonitrile ob-

(1) Asher, S. A.; Johnson, C. R.; Murtaugh, J. *Rev. Sci. Instrum.* **1983**, *54*, 1657–1662. Jones, C. M.; Naim, T. A.; Ludwig, M.; Murtaugh, J.; Flaugh, P. L.; Dudik, J. M.; Johnson, C. R.; Asher, S. A. *TrAC, Trends in Anal. Chem. (Pers. Ed.)* **1985**, *4*, 75–80.

(2) Hudson, B. S.; Mayne, L. C. In "Biological Aspects of Raman Spectroscopy"; T. Spiro, Ed., in press. Kubasek, W. L.; Hudson, B.; Peticolas, W. L. *Proc. Natl. Acad. Sci. U.S.A.*, submitted.

(3) Fodor, S. P. A.; Rava, R. P.; Hays, T. R.; Spiro, T. G. *J. Am. Chem. Soc.* **1985**, *107*, 1520–1529.

(4) Kelly, P. B.; Hudson, B. S. in preparation. Hudson, B.; Mayne, L. "Methods in Enzymology", in press.

(5) Desiderio, R. A.; Gerrity, D. P.; Hudson, B. S. in preparation.

(6) Ziegler, L. D.; Hudson, B. *J. Phys. Chem.* **1984**, *88*, 1110–1116.

(7) Ziegler, L. D.; Hudson, B. S. *J. Chem. Phys.* **1983**, *79*, 1197–1202.

(8) Asher, S. A.; Johnson, C. R. *J. Phys. Chem.* **1985**, *89*, 1375–1379.

(9) Ziegler, L. D.; Hudson, B. *J. Chem. Phys.* **1981**, *74*, 982–992. Gerrity, D. P.; Ziegler, L. D.; Kelly, P. B.; Desiderio, R. A.; Hudson, B. *J. Chem. Phys.*, in press.

(10) Ziegler, L. D.; Hudson, B. S. *J. Chem. Phys.* **1983**, *79*, 1134–1137.

(11) Johnson, C. R.; Ludwig, M.; O'Donnell, S.; Asher, S. A. *J. Am. Chem. Soc.* **1984**, *106*, 5008–5010.

(12) Asher, S. A.; Ludwig, M.; Johnson, C. R. *J. Am. Chem. Soc.*, in press.

(13) Rava, R. P.; Spiro, T. G. *J. Phys. Chem.* **1985**, *89*, 1856–1861.

(14) Johnson, C. R.; Asher, S. A. *Anal. Chem.* **1984**, *56*, 2258–2261. Asher, S. A. *Anal. Chem.* **1984**, *56*, 720–724.

(15) Dudik, J. M.; Johnson, C. R.; Asher, S. A. *J. Phys. Chem.* **1985**, *89*, 3805.

(16) Mayne, L. C.; Ziegler, L. D.; Hudson, B. *J. Phys. Chem.* **1985**, *89*, 3395.

(17) Copeland, R. A.; Dasgupta, S.; Spiro, T. G. *J. Am. Chem. Soc.* **1985**, *107*, 3370–3371.

(18) Copeland, R. A.; Spiro, T. G. *Biochemistry* **1985**, *24*, 4960.

(19) Creed, D. *Photochem. Photobiol.* **1984**, *39*, 537–562. Creed, D. *Photochem. Photobiol.* **1984**, *39*, 563–575.

(20) Bent, D. V.; Hayon, E. *J. Am. Chem. Soc.* **1975**, *97*, 2599–2606. Bent, D. V.; Hayon, E. *J. Am. Chem. Soc.* **1975**, *97*, 2606–2612. Bent, D. V.; Hayon, E. *J. Am. Chem. Soc.* **1975**, *97*, 2612–2619.

(21) Grossweiner, L. I.; Usui, Y. *Photochem. Photobiol.* **1971**, *13*, 195–214. Grossweiner, L. I. *Curr. Top. Radiat. Res. Q.* **1976**, *11*, 141–199.

(22) Mossoba, M. M.; Makino, K.; Riesz, P. *J. Phys. Chem.* **1982**, *86*, 3478–3483.

(23) For example: Finnstrom, B.; Tfibel, F.; Lindquist, L. *Chem. Phys. Lett.* **1980**, *71*, 312–316. Baugher, J. F.; Grossweiner, L. I. *J. Phys. Chem.* **1977**, *81*, 1349–1354.

(24) For example: Grabner, G.; Köhler, G.; Zechner, J.; Getoff, N. *J. Phys. Chem.* **1980**, *84*, 3000–3004.

(25) Dudik, J. M.; Johnson, C. R.; Asher, S. A. *J. Chem. Phys.* **1985**, *82*, 1732–1740.

tained under identical conditions. The maximum likely error in the absolute band frequencies is estimated to be ±4 cm^{-1} for individual spectra and ±6 cm^{-1} for difference spectra.

For the pump–probe experiments the probe beam was split off from the pump beam with a reflective neutral density filter. The probe beam was redirected by two quartz prisms to a second neutral density filter that recombined the probe and pump beams. The increased path length for the probe beam gave a 10-ns delay for the probe pulse relative to the pump pulse.

Results

A typical Raman spectrum of phenolate anion (5 mM in 0.1 M aqueous NaOH) excited at 514.5 nm (CW Ar^+ laser) is shown in Figure 1A, while part B shows a UV resonance Raman spectrum of phenolate excited at 245 nm using a laser pulse energy of 0.15 mJ and an estimated peak power density in the sample of less than 10^7 W/cm^3. Excitation at 245 nm is in resonance with the $^1L_a \leftarrow {}^1A_1$ electronic transition of phenolate (λ_{max} 235 nm, ϵ = 9400 M^{-1} cm^{-1}).[26] The marked changes in the intensity pattern between the spectra in figure 1, parts A and B, result from a selective enhancement of the normal modes vibronically active within the $^1L_a \leftarrow {}^1A_1$ transition. The five normal modes[27] prominent in the resonance-enhanced spectrum are the ν_{8a} C–C ring stretching mode at 1585 cm^{-1}, the ν_{9a} C–H bending mode at 1165 cm^{-1}, the ν_{18a} C–H bending mode at 1020 cm^{-1}, the ν_1 ring-breathing mode at 992 cm^{-1}, and the ν_{12} trigonal ring-breathing mode at 820 cm^{-1}. Each of these modes is also observed in the normal Raman spectrum. No modes occur with resonance excitation that are not observed with preresonance excitation.

Figure 1C shows a spectrum obtained with 245-nm excitation but with tighter focusing of the excitation beam in the sample. We estimate the power density to be greater than 10^{11} W/cm^3. The bands at 1393, 1502, and 1552 cm^{-1} are unique to this high power density excited spectrum and are not observed in either the low power density resonance Raman (Figure 1B) or the normal Raman spectra (Figure 1A). The new features in Figure 1C must be due to either the appearance of a new spectroscopic phenomenon or to the production of a new chemical species. We estimate with ray optics that a pulse energy of 0.1 mJ/pulse results in 200 photons/molecule within the illuminated volume with tight focusing and ca. 0.01 photons/molecule with defocused excitation. Figure 1D shows the UVRR difference spectrum obtained by subtracting the appropriately scaled defocused spectrum (Figure 1B) from the focused spectrum (Figure 1C). The difference spectrum indicates that high power density focused excitation results in new bands at 801, 990, and 1164 cm^{-1} in addition to the easily observed bands at 1393, 1502, and 1552 cm^{-1}. The 990- and 1164-cm^{-1} bands overlap bands present in the normal and defocused resonance Raman spectra of phenolate. The spectrum in Figure 1D derives from a single photoinduced transient species (vide infra), and the bands at 1785, 1963, and 2193 cm^{-1} appear to be combinations of the 801-cm^{-1} band with the other fundamentals. At the same excitation wavelength, the resonance Raman spectrum of phenolate shows combination bands at 1982, 2006 and 2154 cm^{-1} that are assigned to the first overtone of the 992-cm^{-1} mode and to combinations of the 992-cm^{-1} and the 1020- and 1165-cm^{-1} fundamentals.

The Raman bands due to the photoinduced species occur only when the beam is tightly focused and not with low power density excitation. The concentration of the photoinduced species does not increase in time as the sample is recirculated through the laser beam. We were unable to build up observable concentrations of the photoinduced species even by exhaustive illumination of a 15-mL sample over a 4 h period with a total energy of 43.2 J or ~1 photon/molecule. Less than 5% of the phenolate was lost, as monitored by changes in the absorption spectrum. The absolute Raman intensity of the phenolate Raman bands and the ratio of phenolate Raman intensity to photoinduced species Raman intensity did not change measurably during photolysis with focused high power density excitation. Even after 4 h in the beam no Raman bands due to the photoinduced species are detected with low power density excitation. *p,p*-Biphenol, a major photoproduct of the UV photolysis of phenol, shows a resonance Raman spectrum different from that of the photoinduced species.[28] These results indicate that the photoinduced species is produced transiently and does not build up as a permanent photoproduct.

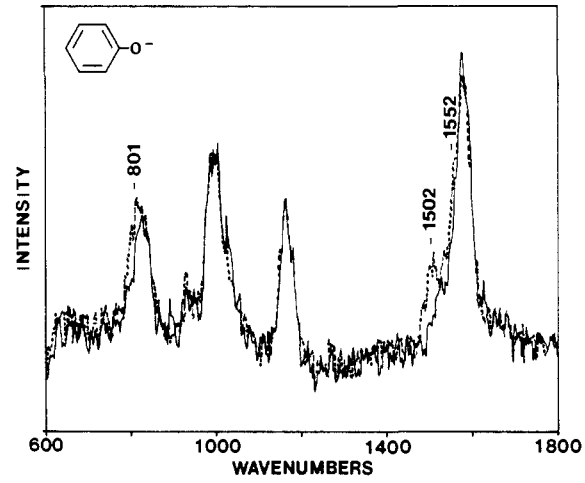

Figure 2. Pump–probe experiment at 245 nm of a 5 mM phenolate solution (pH 12). The solid spectrum is obtained from the 0.005-mJ probe pulse only. The dashed spectrum was obtained from the probe pulse when it was preceeded by a 0.02-mJ pump pulse 10 ns prior to the arrival of the probe pulse. The intensifier of the Reticon detector was gated on by a Princeton Applied Research Model 1302 fast pulser for a 10-nsec interval following the pump probe. This interval bracketed the probe pulse. Spectral bandpass = 25 cm^{-1}.

Figure 2 shows a pump–probe experiment which demonstrates that the photoinduced transient has a lifetime longer than 10 ns and that the new bands do not derive from nonlinear optical processes occurring during the 4-ns laser pump pulse. In this experiment the Reticon detector was active only during the probe pulse. The solid curve was obtained by using only the probe pulse, while the dashed spectrum was obtained when a 4-ns pump pulse of 4 times the probe pulse power was incident in the sampling volume 10 ns prior to the probe pulse. Prior illumination by the pump pulse results in Raman intensity increases at frequencies that correspond to the three most intense bands of the transient at 801, 1502, and 1552 cm^{-1}. Raman scattering from the pump pulse alone results in a spectrum with the same relative intensities of transient and phenolate bands. Thus, little decay of the transient occurs during the 10-ns time interval. Because of experimental limitations, we were unable to examine the transient at delay intervals significantly longer than 10 ns.

Similar photoinduced transient spectra are observed for tyrosinate solutions as shown in Figure 3. Figure 3A shows the normal Raman spectrum of tyrosinate excited with a CW laser at 488 nm. Figure 3B shows a UVRR spectrum of tyrosinate excited at 245 nm with defocused pulsed excitation. Only the four fundamentals that are most prominent in the normal Raman spectrum of tyrosinate (Figure 3A) are significantly enhanced with resonance excitation in the $^1L_a \leftarrow {}^1A_1$ electronic transition. These four fundamentals are the ν_{8a} C–C ring-stretching mode at 1599 cm^{-1}, the ring-breathing mode characteristic of para-substituted benzenes at 1207 cm^{-1}, the ν_{9a} C–H bending mode at 1174 cm^{-1}, and the ν_1 ring-breathing mode at 852 cm^{-1}. Also enhanced is a band at 831 cm^{-1} that has been assigned to the first overtone of ν_{16a}, an out-of-plane ring-bending mode.[13] This overtone is in Fermi resonance with the ν_1 mode from which it is unresolved in the UVRR spectrum shown here. As for phenolate, new bands appear when the laser beam is tightly focused (Figure 3C). The spectrum of the transient species (Figure 3D) shows a pattern of bands similar to that of the phenolate transient but with some frequency shifts. The three most prominent tyrosinate transient

(26) Jaffe, H. H.; Orchin, M. "Theory and Applications of Ultraviolet Spectroscopy"; Wiley: New York, 1962, p 257.

(27) The modes are numbered with Wilson's numbering for benzene modes. Wilson, E. B., Jr. *Phys. Rev.* **1934**, *45*, 706.

(28) Beck, S. M.; Brus, L. E. *J. Chem. Phys.* **1982**, *76*, 4700–4704.

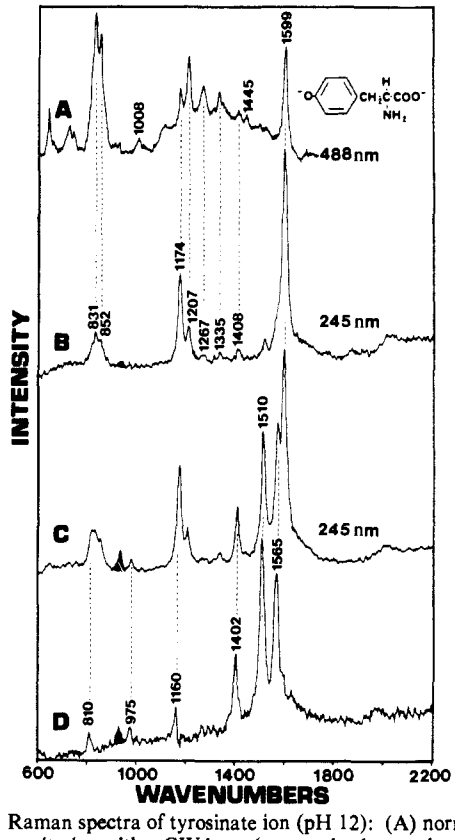

Figure 3. Raman spectra of tyrosinate ion (pH 12): (A) normal Raman at 488-nm excitation with a CW laser (a water background spectrum has been subtracted, power = 900 mW, spectral bandpass = 2.5 cm^{-1}, the tyrosinate concentration is 100 mM); (B) UVRR spectrum of a 5 mM tyrosinate solution at 245-nm excitation using a 20-Hz Nd–Yag laser at 3-mW average power (the laser beam was focused above the sample); (C) same conditions as B but with the laser beam focused in the sample; (D) spectrum of the tyrosinate photoinduced transient obtained as the difference spectrum between B and C. Perchlorate ion is indicated by shading. Spectral bandpass = 12 cm^{-1}.

bands occur at 1402, 1510, and 1565 cm^{-1}. Other transient bands are seen in the difference spectrum at 810, 975, and 1160 cm^{-1}.

The photoinduced transient of phenolate is generated with all excitation wavelengths between 217–270 nm. This includes excitation in the lower energy $^1L_b \leftarrow {}^1A_1$ electronic transition. High power density excitation of phenol and tyrosine solutions at pH 7 also results in the formation of new peaks due to a transient species. The spectra of the transients observed for phenol and tyrosine solutions are identical with those observed for phenolate and tyrosinate, respectively.

The relative Raman intensities of phenolate, tyrosinate, and their transients depend upon the incident laser intensity. Figure 4 shows the relative laser power density dependence of the Raman intensities of bands occurring in spectra from a phenolate solution with 235-nm excitation and from a tyrosinate solution with 245-nm excitation. Neutral density filters were used to attenuate the laser-power density in order to maintain the excitation beam position, divergence, and focusing in the sample. The data are plotted either as absolute Raman intensities or as the ratio of Raman intensity to the perchlorate internal standard intensity. As expected, the absolute Raman intensity of perchlorate depends linearly on incident laser intensity (Figure 4, parts A and B). The intensities of the two most intense bands of phenolate and tyrosinate and their transients are plotted in Figure 4.

The 235-nm excited phenolate spectra show that both the 1165 and 1585 cm^{-1} phenolate peaks as well as the 1393 and 1502 cm^{-1} transient peaks increase in intensity as the laser intensity increases. The intensity of the phenolate peaks extrapolate at low laser power to zero, as expected. Their intensities appear to increase linearly up to ca. 20% of the maximum laser power used. The intensity then increases more slowly, showing clear saturation by the 50% power level. The power-density dependence of the peaks of the

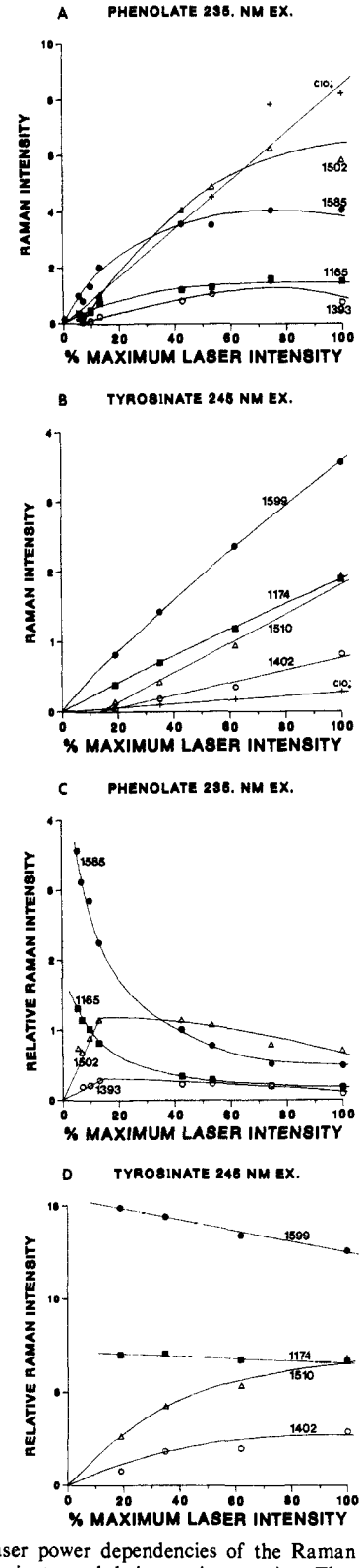

Figure 4. Laser power dependencies of the Raman scattering from phenolate, tyrosinate, and their transient species. The phenolate data is for 235-nm excitation, and the tyrosinate data is for 245-nm excitation. The maximum laser power at each wavelength was 4 mW. A and B show the dependency of the absolute Raman intensity, and C and D show the dependency of the relative Raman intensity. The relative Raman intensities are the ratio of the Raman intensity of the peak to the intensity of perchlorate, the internal standard. The 1502- and 1393-cm^{-1} bands from the phenolate solution spectra and the 1510- and 1402-cm^{-1} bands from the tyrosinate solution spectra are due to the transient species. These are indicated by the open markers. The other bands, indicated by solid markers, are due primarily to the parent compounds, phenolate or tyrosinate. The phenolate and tyrosinate solutions were 5 mM at pH 12. The perchlorate concentration was 1.0 M in the phenolate solution and 0.2 M in the tyrosinate solution.

Table I. Raman Fundamentals of Phenol, Tyrosine, Tryptophan, and Their Photoinduced Transient Species[a]

	ν_{12}	ν_1	ν_{18a}	ν_{9a}		ν_{7a}	ν_{14}	ν_{19b}	ν_{8a}	ref
toluene	786	1005	1031			1213			1604	*b*
phenol	811	996	1021	1170		~1260 (w,br)			1598	*b*
phenolate	820	992	1020	1165		1265 (w)	1318 (w)		1585	*b*
phenolate transient		801	990	1164		1502		1393	1552	*b*
phenoxy radical	840		990	1157		1505	1331	1398		32,*c*
tyrosine		853		1180	1210	1263 (w)			1617	13,*b*
tyrosinate		852		1174	1207	1267 (w)		1335 (w)	1599	*b*
tyrosinate transient		810	975	1160		1510		1402	1565	*b*

tryptophan	759	881	1008	1125	1155	1232	1340	1352	1458		1549	1617	*b*
tryptophan transient	753		1008	1125	1170	1233	1283	1328	1434	1522	1593	1646	*b*

[a] The fundamentals assigned here are those observed with UV excitation (typically 235 and 245 nm) in aqueous solution except for toluene, which is in acetonitrile. [b] This work. [c] Data from ref 32 is for excitation in the 400-nm region.

transient does not extrapolate to zero at zero laser power; however, the intensity appears to increase linearly with laser power until ca. 70% power, where the intensity begins to level off and then decrease.

Figure 4B shows similar data for tyrosinate except that the power density in the sample is below that required for saturation of the Raman intensities. Both the transient and tyrosinate peaks appear to increase in intensity linearly with laser power; however, the intensity of the Raman bands of the transient does not extrapolate to 0 at zero incident power. Although it is reasonably clear in Figure 4, parts A and B that the transient peak intensities do not extrapolate to zero at zero laser power, it is obviously easy to choose a set of laser powers that extrapolate to zero within the signal-to-noise ratio of the data. Indeed, the lowest laser intensity data, which are the most robust indicators of the lack of extrapolation to zero, have the poorest signal-to-noise ratios. If one uses a linear intensity dependence as a criteria for the presence of only linear resonance Raman scattering from a ground-state species, these data would lead to the incorrect conclusion that the peaks of the transient derive from linear Raman scattering from ground-state phenolate and tyrosinate.

Figure 4, parts C and D give a clearer insight into the intensity dependence of the Raman bands of the ground and transient species; the ratio of intensities of these bands to the internal standard ClO_4^- intensity effectively cancels the typical Raman linear incident intensity dependence. Thus, Figure 4C demonstrates a rapid exponential-like decrease in intensity of the phenolate peaks. In contrast, the transient peak relative intensities increase linearly with incident laser intensity for intensities below 20% of the maximum. Above 20% the increase saturates and drops off. The linear increase in the transient relative peak intensities demonstrates the quadratic dependence of the transient peak intensities on incident excitation power density. Figure 4D shows similar data for tyrosinate with an excitation wavelength and a range of laser-power densities for which saturation is not as evident. Thus, linear behavior dominates below 40% relative laser power density, and the power-density dependence of the transient peaks is obviously quadratic. The use of the incident laser intensity dependence of relative Raman intensities as a clear monitor of the formation of transient species requires measurements of spectra at appropriately low laser powers. For example, the Figure 4C data obtained between 30% and 100% laser intensity could be construed to indicate that the relative Raman intensities are almost independent of laser intensity.

The saturation and subsequent absolute and relative intensity decreases observed for the Raman bands of the transient at high power densities indicate that new species or processes are occurring. Either the concentration of the transient species is decreasing or new optical processes occur that effectively compete with resonance Raman scattering from the transient.

The appearance of transient species is not limited to easily oxidized molecules like phenol and tyrosine. Normal Raman and resonance Raman spectra of tryptophan excited at 488 and 235 nm are shown in Figure 5, parts A and B. A 235-nm excited spectrum at higher power density is shown in Figure 5C. Figure 5D shows the difference spectrum (C–B). As with phenolate and tyrosinate, new bands are observed with high power density ex-

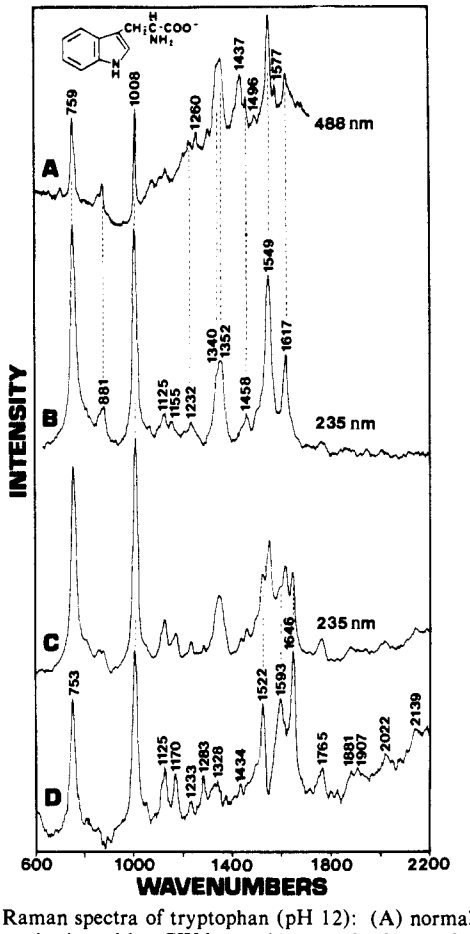

Figure 5. Raman spectra of tryptophan (pH 12): (A) normal Raman at 488-nm excitation with a CW laser. (A water background spectrum has been subtracted, power = 900 mW, spectral bandpass = 2.5 cm^{-1}, the tryptophan concentration is 100 mM); (B) UVRR spectrum of a 5 mM tryptophan solution at 235-nm excitation using a 20-Hz Nd–Yag laser at 5.5 mW average power (the laser beam was focused above the sample); (C) same conditions as B but with the laser beam focused at the sample; (D) spectrum of the tryptophan transient obtained as the difference spectrum between B and C. Spectral bandpass = 13 cm^{-1}.

citation. The new features that occur at 1522, 1593, and 1646 cm^{-1} are accompanied by additional features in the combination and overtone region (>1700 cm^{-1}). The spectrum of the transient species shown in Figure 5D is very similar to that of tryptophan except for small differences in frequencies and changes in relative intensities. Overtones and combinations involving the 753, 1008, and 1125 cm^{-1} modes are observed at 1765, 1881, 1907, 2022, 2139, and 2255 cm^{-1} (not shown). The Raman data for tryptophan, tyrosinate, phenol, phenolate and their respective photoinduced transient species are summarized in Table I.

Discussion

A primary event in the photochemistry of aromatic molecules in the condensed phase is the photoejection of an electron into

the solvent.[29] The subsequent formation of permanent photoproducts involves free radical reactions that follow the initial photoionization process. Evidence for this process is overwhelming for phenol, which is relatively easily photooxidized, as well as for the aromatic amino acids and other related compounds.[19]

Photoionization is particularly important in the photochemistry of phenol and tyrosine in polar solvents such as water.[30] The quantum yields for electron photoejection from aqueous phenol have been reported as 0.03–0.32, depending upon the method of measurement and whether pulsed or CW excitation sources were used.[19] A recent flash photolysis study using 27-ps pulses of 265-nm light showed that the photoionization of phenolate ion has a quantum yield of 0.37 for electron photoejection, is mostly monophotonic, and is essentially instantaneous on the 27-ps time scale.[31] Thus, the phenoxy, tyrosyl, and tryptophanyl radicals are candidates for the photochemical transients we observe with UV excitation. Indeed, recent resonance Raman studies of phenoxy radical give similar spectra to those we observe for the transient obtained in phenolate solutions with high power density excitation. Tripathi and Schuler studied the resonance Raman spectrum of phenoxy radical produced with pulse radiolysis by exciting near 400 nm within the 0–0 absorption band of the lowest electronic transition of phenoxy radical.[32,33] The phenoxy radical Raman bands that were selectively enhanced with 400-nm excitation are similar in frequency to bands observed in our study. We have adopted the notation and concur in the assignments of Tripathi and Schular which are based in part on spectra also obtained for phenoxy-2,4,6-d_3 and phenoxy-d_5.[32b] Table I lists the bands observed by Tripathi and Schuler as well as the bands we observe for the transient.

The most prominent band in the 400-nm excitated spectrum of phenoxy radical is at 1505 cm^{-1} and is assigned to the ν_{7a} vibration which has significant C–O stretching character. Similarly, our phenolate and phenol transient shows its strongest band at 1502 cm^{-1}. Several other bands observed with 400-nm excitation for phenoxy radical have complimentary features in the transient we obtain with UV excitation below 250 nm. These bands occur at 1393, 1164, and 990 cm^{-1}. Bands reported at 840 and 1331 cm^{-1} with 400-nm excitation are not seen in the transient with UV excitation, presumably because they are not resonance-enhanced with 245-nm excitation. Instead new bands appear at 1552 and 801 cm^{-1} with UV excitation. Tripathi and Schuler remarked on the notable absence of any band assignable to ν_8 in their 400-nm excited phenoxy spectrum. We assign the 1552-cm^{-1} band to the ν_8 vibration. We tentatively assign the 801-cm^{-1} feature to the ν_1 ring-breathing mode. The similar features observed in this report and in that of Tripathi and Schuler's work identifies the photochemical transient as phenoxy radical. The difference observed between 400-nm and UV excitation below 250 nm reflects the different resonant electronic transitions of phenoxy. Transient absorption studies have shown that phenoxy radical strongly absorbs throughout the UV spectral region[20] and several electronic transitions are expected in the 200–400-nm spectral region.

The respective transients in the phenol(ate), tyrosine(ate), and tryptophan spectra are reasonably assigned to phenoxy, tyrosyl, and tryptophanyl radicals. The observation that the same transient spectrum is observed for phenol (pH 7) and phenolate (pH 12) (as well as for tyrosine and tyrosinate) further supports the assignment of the transient as phenoxy radical. The pK_a of $PhOH^+$ is −2.0.[34] Thus, phenol and phenolate must both produce the neutral phenoxy radical at any normal aqueous pH value. Proton dissociation from $PhOH^+$ will be very rapid in aqueous solution. Photoionization is an important photophysical process for tryptophan with excitation wavelengths shorter than ≈286 nm. Typical quantum yields for photoionization of tryptophan in water are 0.08 at 265 nm and 0.32 at 250 nm with sharp increases toward shorter wavelengths.[35]

Resonance Raman spectra of the tyrosyl and tryptophanyl radicals have not been previously reported at any excitation wavelength. Table I compares the Raman bands of phenol, phenolate, tyrosine, tyrosinate, tryptophan, and their radical photoproducts. Useful comparisons can be made between the enhancement patterns of the species shown in Table I. Toluene is included since the effective symmetry is the same as phenol and its UV Raman spectrum has been well characterized.[10,36] Typically ν_{8a} is strongly enhanced in the resonance Raman of benzene derivatives throughout the region of the $^1L_a \leftarrow {}^1A_1$ and $^1L_b \leftarrow {}^1A_1$ absorption bands. This mode also predominates in phenol and phenolate with UV excitation (detailed excitation profiles of phenol and phenolate will be reported elsewhere).[37] Thus, the general features of the UVRR spectra of toluene, phenol, and phenolate are remarkably similar despite large differences in their UV absorption spectra.

A unique feature observed in the excitation profile of phenolate in the $^1L_a \leftarrow {}^1A_1$ absorption band at 235 nm is the lack of activity of ν_{7a} (1265 cm^{-1}), which involves C–O stretching. However, this mode is enhanced in resonance with the $^1L_b \leftarrow {}^1A_1$ transition and shows enhancement at energies above the $^1L_a \leftarrow {}^1A_1$ transition. In contrast, the UVRR spectrum of phenoxy radical shows strong enhancement of ν_7 at all UV excitation wavelengths studied. Also strongly enhanced in phenoxy radical is a peak at 1393 cm^{-1}, which is assigned to ν_{19b}.[32] This mode is not obviously enhanced in toluene, phenol, or phenolate. A similar comparison can be made for tyrosine and tyrosyl radical; tyrosyl radical shows strong enhancement of ν_{7a} at 1510 cm^{-1} and ν_{19b} at 1402 cm^{-1}.

The electronic states shift to lower energy in the radical species compared to those of phenol, tyrosine, and tryptophan. Because of this energy shift, the electronic state in resonance at any particular excitation wavelength would be different for the radical and its parent compound. This may explain why phenoxy radical and tyrosyl radical have enhancement patterns atypical of small aromatic compounds with UV excitation above 217 nm.

On the other hand tryptophan and tryptophanyl radical have similar Raman spectra with similar enhancement patterns. The different enhancement patterns between phenol and phenoxy may reflect fundamental differences between the nature of the π orbitals involved in the electronic transitions. In the phenoxy radical substantial unpaired electron density resides on the oxygen atom[38] and the electronic transitions have considerable charge-transfer character. This is reflected in the strongly enhanced C–O stretching vibration. In phenol the ring-stretching mode, ν_8, is the most strongly enhanced with UV excitation, indicating that the geometry changes of the excited state are mainly confined to the ring itself. For tryptophanyl radical the unpaired electron density must reside on the indole ring; there is no oxygen exo to the ring on which to distribute electron density. As a result, the UVRR spectra of tryptophan and tryptophanyl radical are similar. UVRR spectroscopy may become an important technique for studying free radicals species.

(29) Joschek, H.-I.; Grossweiner, L. I. *J. Am. Chem. Soc.* **1966**, *88*, 3261–3268.
(30) Zechner, J.; Köhler, G.; Grabner, G.; Getoff, N. *Can. J. Chem.* **1980**, *58*, 2006–2010.
(31) Mialocq, J.-C.; Sutton, J.; Goujon, P. *J. Chem. Phys.* **1980**, *72*, 6338–6345.
(32) (a) Tripathi, G. N. R.; Schuler, R. H. *Chem. Phys. Lett.* **1983**, *98*, 594–596. (b) Tripathi, G. N. R.; Schuler, R. H. *J. Chem. Phys.* **1984**, *81*, 113–121.
(33) Several other reports on the resonance Raman of phenoxy radical should be noted. Reference 28 reports the ~400-nm resonance Raman spectrum of phenoxy radical produced by flash photolysis with a 265-nm laser pulse. Tripathi and Schuler[32] have indicated that their qualitative results are in agreement with those of Beck and Brus[28] but that the Raman frequencies reported by the latter group are probably in error. Another report of the Raman spectrum of phenoxy radical produced chemically (Shindo, H.; Hiraishi, J. *Chem. Phys. Lett.* **1981**, *80*, 238–241) does not agree with ref 28, 32, or the present work.
(34) Dixon, W. T.; Murphy, D. *J. Chem. Soc., Faraday Trans. 2* **1976**, *72*, 1221–1230.
(35) Amouyal, E.; Bernas, A.; Grand, D. *Photochem. Photobiol.* **1979**, *29*, 1071–1077. Amouyal, E.; Bernas, A.; Grand, D.; Mialocq, M.-C. *Faraday Discuss. Chem. Soc.* **1982**, *74*, 147–160.
(36) Ziegler, L. D.; Albrecht, A. C. *J. Chem. Phys.* **1979**, *70*, 2634–2643. Ziegler, L. D.; Albrecht, A. C. *J. Chem. Phys.* **1979**, *70*, 2644–2651.
(37) Johnson, C. R.; Asher, S. A. to be submitted.
(38) Stone, T. J.; Waters, W. A. *J. Chem. Soc.* **1964**, 213–218.

Initial studies of the UV Raman spectra of aromatic amino acids with focused excitation (i.e., the experimental arrangement that gives the optimal signal-to-noise ratio in Raman measurements) have resulted in published UV resonance Raman spectra that mistakenly assign tyrosyl radical peaks to the ground-state tyrosine and tyrosinate species.[11,13] The improper assignments obviously lead to incorrect conclusions regarding vibronic coupling in tyrosine excited states. Further, preliminary excitation profiles of the aromatic amino acids that we reported to show detailed structure are now accounted for by contributions from the radical transients formed and by saturation effects.[39] The incorrect identification of tyrosyl radical Raman bands as resonance-enhanced tyrosine peaks indicates the potential artifacts possible in pulsed-UV resonance Raman excitation and clearly illustrates that care (low power densities) is required to avoid such artifacts. It is especially important to realize that the power-density dependence of radical detection may be quadratic in power density (vide infra) but experimentally appears close to linear in intensity if insufficient care is taken in the power-dependence measurements.

The quadratic incident power Raman intensity dependence from a photochemical intermediate produced by a monophotonic process can be easily accounted for by a simple mechanism where incident photons produce either the photochemical transient, T, or Raman intensity from the transient (I_T) or from the original precursor (I_P). P, the precursor, is either phenolate or tyrosinate.

$$I_P \xleftarrow[\sigma_P]{\nu} P \xrightarrow[\sigma_A]{\nu} T \xrightarrow[\sigma_T]{\nu} I_T$$

where σ_A and σ_P and σ_T are the cross sections for the photochemical reaction and the cross sections for Raman scattering from P and T, respectively. The units for the cross section as used here are cm^2/mol. The intensity at time t for the laser pulse can be described with the normalized temporal band shape function $L(t)$ and the total integrated power within the pulse, I_0.

$$I(t) = I_0 L(t)$$

The rate of formation of the transient species is

$$dT/dt = \sigma_A I(t) P = -dP/dt$$

Thus the concentration of phenolate or tyrosinate at any time during the laser pulse is

$$P(t) = P_0 e^{-\sigma_A \int_0^t I(t)\, dt}$$

where P_0 is the initial concentration of P. This assumes that no T decays back to P during the 4-ns laser pulse. Since the sampled volume is replenished between laser pulses we can independently consider each laser pulse. The experimental result is just the sum of the independent identical processes occurring with each pulse. The total amount of T formed at time t is

$$T(t) = P_0[1 - e^{-\sigma_A \int_0^t I(t)\, dt}]$$

The experimental observable, $\bar{I}_T$ or $\bar{I}_P$, is the Raman intensity derived from a unit sample volume integrated over the time of the entire laser pulse.

$$\bar{I}_t = \int_0^\infty I_T(t)\, dt = \int_0^\infty \sigma_T I(t) T(t)\, dt$$

$$\bar{I}_P = \int_0^\infty I_P(t)\, dt = \int_0^\infty \sigma_P I(t) P(t)\, dt$$

where $I_T(t)$ and $I_P(t)$ are the Raman scattered intensities at time t.

$$\bar{I}_T = \sigma_T P_0 I_0 \left[\int_0^\infty L(t)\, dt - \int_0^\infty L(t) e^{-\sigma_A I_0 \int_0^t L(t)\, dt}\, dt \right]$$

$$\bar{I}_P = \sigma_P P_0 I_0 \int_0^\infty L(t) e^{-\sigma_A I_0 \int_0^t L(t)\, dt}\, dt$$

remembering that $\int_0^\infty L(t)\, dt = 1$ and substituting $y(t) = \int_0^t L(t)\, dt$ to facilitate the integration, one obtains

$$\bar{I}_T = \sigma_T P_0 I_0 \left[1 + \frac{1}{\sigma_A I_0} (e^{-\sigma_A I_0} - 1) \right]$$

$$\bar{I}_P = \frac{\sigma_P P_0}{\sigma_A} [1 - e^{-\sigma_A I_0}]$$

When $\sigma_A I_0 \ll 1$, the extent of photochemistry is small and

$$\bar{I}_T \approx \sigma_A \sigma_T P_0 I_0^2 / 2$$

This expression predicts a quadratic power dependence up to those power densities where the first three terms in the series expansion of the exponential represents a good approximation to the expression. As the laser-power density increases, cubic and higher order terms begin to contribute and eventually predominate. The low power density data for phenoxy and tyrosyl radical shown in Figure 4 are consistent with the expectation of a quadratic intensity dependence and give new experimental evidence that formation of phenoxy radical occurs by a one-photon process (at least at high pH).[20] In contrast, however, to the higher than quadratic power-density dependence expected at high power densities, the data in Figure 4 indicate saturation of the quadratic intensity dependence and show an inverse relationship to laser-power density at high powers. This is a clear indicator of further photophysical or optical processes at high laser-power densities.

At low power densities the Raman intensity of the precursors, phenolate and tyrosinate, should follow a power dependence of

$$\bar{I}_P \cong \sigma_P P_0 I_0 [1 - \sigma_A I_0 / 2]$$

The relative Raman intensity, S_p, follows the expression

$$S_P \approx \frac{\sigma_P P_0}{\sigma_c C_0} \left[1 - \frac{\sigma_A I_0}{2} + \frac{\sigma_A^2 I_0^2}{3!} - \ldots \right]$$

σ_c and C_0 are the Raman cross section and the concentration of the internal standard. The intercept of the relative Raman intensity vs. laser intensity plot is $\sigma_P P_0 / \sigma_c C_0$. At low laser powers the slope is related to the photochemical cross section for production of the radical. This linear behavior is similar to that observed in Figure 4. The linear decrease in the relative Raman intensity is predicted to level off as the higher order terms contribute at higher power density. These expectations are seen experimentally in Figure 4.

Conclusions

The results obtained here contain several clear messages to those doing UVRR spectroscopy with pulsed-laser sources. One should always expect that laser excitation in the UV with pulsed sources will produce detectable transient species or saturation effects unless care is taken to avoid high power densities. Several Raman bands of tyrosine have already been misassigned in the literature because insufficient precautions were taken to avoid transient production. In particular, any Raman bands observed with UV excitation that cannot be correlated to even weak bands in the normal Raman spectra should be viewed with suspicion. Note that the appearance of a band only in resonance is not unusual (we recently reported such a case[15]) but must be carefully verified. The standard test for linear Raman effects, a study of the Raman intensity as a function of laser intensity, can lead to deceptive results. A combination of photochemistry and saturation can lead to power-dependence curves that appear linear over a fairly wide range of powers but that over a smaller or larger power range would show a higher order power dependence.

We have also observed saturation effects in UV Raman excitation profile measurements that dramatically altered the relative intensities of the analyte to the internal standard. These saturation effects can make accurate excitation profile measurements extraordinarily difficult. Apparently, the absorption saturates along the laser beam path through a part of the height of the sample volume that is imaged into the entrance slit of the spectrometer.

(39) Asher, S. A.; Johnson, C. R., Ludwig, M.; Dudik, J. M. *Proc. IXth Int. Conf. Raman Spectrosc.* **1984**, 430.

For a sample of high optical density, the height of the sample volume is less than that imaged into the spectrometer and saturation does not result in a decrease in intensity of the analyte bands but only increases the Raman intensity from the transparent solvent and internal standard in the bleached sampling volume.

Note Added in Proof. Recently we reassigned the ca. 1000 cm^{-1} and 800 cm^{-1} substituted benzene Raman peaks to the ν_{12} and ν_1 modes of benzene, respectively. We have avoided dwelling on this reassignment in this paper because it would confuse comparisons with data cited by other workers. Details on this reassignment are found in ref 12.

Acknowledgment. We gratefully acknowledge partial support of this work from NIH grant 1R01GM30741-04. Sanford A. Asher is an Established Investigator of the American Heart Association; this work was done during the tenure of an Established Investigatorship of the American Heart Association and with funds contributed in part by the American Heart Association, Pennsylvania affiliate.

Registry No. Phenol, 108-95-2; tyrosine, 60-18-4; tryptophan, 73-22-3.

Cadmium-113 Shielding Tensors of Cadmium Compounds. 3. Single-Crystal Studies on Cadmium Glycinate Monohydrate and Cadmium Dinitrato Bis(1,1,3,3-tetramethyl-2-thiourea)

Robert S. Honkonen,† Paul S. Marchetti, and Paul D. Ellis*

Contribution from the Department of Chemistry, University of South Carolina, Columbia, South Carolina 29208. *Received June 11, 1985*

Abstract: Cadmium glycinate monohydrate and cadmium dinitrato bis(1,1,3,3-tetramethyl-2-thiourea) have been investigated by single-crystal oriented ^{113}Cd NMR. The cadmium shielding tensor elements for the two sulfur–four oxygen system in $Cd(C_5H_{12}N_2S)_2(NO_3)_2$ are −340, +308, and +327 ppm for σ_{11}, σ_{22}, and σ_{33}, respectively. The 438 ppm anisotropy and the extreme magnitude of σ_{11} are discussed in terms of cadmium–sulfur and cadmium–nitrate interactions. The orientation of the shielding tensor is in agreement with previous results for oxo–cadmium crystals. The ^{113}Cd shielding tensor elements for $Cd(NH_2CH_2CO_2)_2 \cdot H_2O$ were determined to be −116, +200, and +256 ppm relative to solid $Cd(ClO_4)_2$. The orientation of the tensor in this two nitrogen–four oxygen system was found to be dominated by the glycinate chelate moieties.

Substitution of Cd^{2+} for Ca^{2+} in parvalbumin,[1] troponin,[2,3] calmodulin,[4] insulin,[5] and concanavalin A[6] places cadmium in an all-oxygen coordination environment. The ^{113}Cd NMR spectroscopy of these cadmium-substituted metalloproteins gives rise to anomalously shielded isotropic chemical shifts (for a review of NMR of calcium-binding proteins, see ref 7). Because of our interest in the development and utilization of cadmium magnetic resonance as a probe of calcium sites in the muscle proteins troponin and calmodulin, we have undertaken an extensive investigation of the structural factors responsible for this characteristic cadmium chemical shielding. In particular we have been interested in how cadmium–oxygen bond length dispersion and variation in the source of oxygen ligands are manifest in the magnitude and orientation of individual shielding tensor elements. Previous solution and solid-state work[8-10] on oxo–cadmium model compounds indicates that the isotropic average of the cadmium shielding tensor is not sufficiently discriminating to establish structure–shift correlations.

Preliminary single-crystal oriented ^{113}Cd NMR of seven oxo–cadmium compounds has demonstrated four tensor element–structure correlations.[11,12] First, tensor elements of comparable magnitude have similar orthogonal environments. Second, the least shielded tensor element is aligned nearly orthogonal to planes containing water oxygens. Third, if the cadmium coordination sphere is devoid of water oxygens, then the least shielded element is oriented to maximize the short cadmium–oxygen bond shielding contribution. Fourth, the most shielded tensor element is nearly perpendicular to the longest cadmium–oxygen bond.

These data suggest the following interpretation of cadmium chemical shielding. The isolated closed-shell Cd^{2+} ion is the most shielded species possible. Any perturbation of this configuration via bond formation results in a "deshielding" of the cadmium nucleus. Long cadmium–oxygen bonds, typically associated with poor ligands such as nitrate and sulfate, indicate weak bonding interactions. Tensor elements reflecting contributions from these types of interactions are therefore shielded relative to the hexaaquo species, $Cd(ClO_4)_2$. Conversely, more covalent cadmium–nitrogen and cadmium–sulfur bonding interactions represent greater perturbations of the closed-shell configuration. Tensor elements reflecting shielding contributions from these ligands are therefore expected to fall in the deshielded region of the chemical shift range.

In order to refine these arguments, the orientation of the ^{113}Cd shielding tensor in single cyrstals of cadmium glycinate monohydrate and cadmium nitrate tetramethylthiourea was determined. For the establishment of tensor element–structure correlations, these two crystals represent excellent two nitrogen–four oxygen and two sulfur–four oxygen systems. The orientation of the least

† Present address: Eastern Research Center, Stauffer Chemical Company, Dobbs Ferry, NY, 10522.

(1) Drakenberg, T.; Lindman, B.; Cavé, A.; Parello, J. *FEBS Lett.* **1978**, *92*, 346.
(2) Forsén, S.; Thulin, E.; Lilja, H. *FEBS Lett.* **1979**, *104*, 123.
(3) Ellis, P. D.; Strang, P.; Potter, J. D. *J. Biol. Chem.* **1984**, *259*, 10348.
(4) Forsén, S.; Thulin, E.; Drakenberg, T.; Krebs, J.; Seamon, K. *FEBS Lett.* **1980**, *117*, 189.
(5) Sudmeier, J. L.; Bell, S. J.; Storm, M. C.; Dunn, M. F. *Science (Washington, D.C.)* **1981**, *212*, 560.
(6) Palmer, A. R.; Bailey, D. B.; Behnke, W. D.; Cardin, A. D.; Yang, P. P.; Ellis, P. D. *Biochemistry* **1980**, *19*, 5063.
(7) Vogel, H. J.; Drakenberg, T.; Forsén, S. In "NMR of Newly Accessible Nuclei"; Laszlo, P., Ed.; Academic Press: New York, 1983; Vol. 1, p 157.
(8) Ellis, P. D. *Science (Washington, D.C.)* **1983**, *221*, 1141.
(9) Ellis, P. D. In "The Multinuclear Approach to NMR Spectroscopy"; Lamberg, J. B., Riddell, F. B., Eds.; D. Reidel: Boston, 1983; p 457.
(10) Armitage, I. M.; Boulanger, Y. In "NMR of Newly Accessible Nuclei"; Laszlo, P., Ed.; Academic Press: New York, 1983, Vol. 2, p 337.
(11) Honkonen, R. S.; Doty, F. D.; Ellis, P. D. *J. Am. Chem. Soc.* **1983**, *105*, 4163.
(12) Honkonen, R. S.; Ellis, P. D. *J. Am. Chem. Soc.* **1984**, *106*, 5488.

0002-7863/86/1508-0912$01.50/0